2026 IEEE/SICE International Symposium on System Integration (SII)
January 11-14, 2026. Cancún, México

Discrete Element Method Study of Hopping on Granular Media to Develop Analytical Model for Hopping Robot Design

Rio Makino[1] and Takao Maeda[2]

Abstract— **Small-scale planetary exploration missions have been attracting significant attention in recent years. To maximize the scientific return from these missions, compact rovers are required. Hopping is a promising locomotion strategy for achieving both high traversability and compactness. However, hopping on soft granular terrain such as regolith is challenging due to significant energy dissipation into the medium. The dynamics of sand flow during hopping are not yet well understood, especially for diagonal trajectories. This study investigates sand behavior during diagonal hopping using the Discrete Element Method (DEM) simulations. We focused on how the added-mass effect and the effective friction coefficient vary with the hopping angle. Our results revealed a fundamental trade-off: shallower hopping angles decrease the inertial resistance from added mass, yet simultaneously increase effective friction, which enhances propulsive force. In addition, we applied the observed friction behavior to hopping simulations and confirmed its effectiveness. A reduced-order simulation incorporating this variable friction behavior reproduced the experimental hopping efficiency (0.31 in simulation versus 0.35 in experiment) more accurately than the fixed-friction model. These insights provide a physical basis for the development of more efficient hopping mechanisms for future planetary rovers.**

I. INTRODUCTION

In recent years, there has been a growing trend in planetary exploration toward using small, cost-efficient landers. Advances in technology are enabling precise landings in scientifically valuable but challenging terrains, a capability demonstrated by the success of the Japanese SLIM lander [1]. To explore these landing sites, small rovers that can be easily deployed by such landers are required. In addition, a swarm of small rovers can outperform a larger rover in terms of coverage and time efficiency, by applying swarm robotics [2]. However, the traversability of small rovers is limited. As the rovers become smaller, obstacles appear larger relative to their size. One way to improve traversability is to employ hopping motion. Several hopping robots have been applied to space exploration [3], [4]. In addition to space exploration, many kinds of hopping robots have been developed [5], [6], [7], [8], [9], [10], [11]. Hopping motion offers two main advantages over traditional wheeled or tracked rovers. First, hopping rovers can traverse obstacles significantly larger than themselves. The obstacle-clearing capability of wheeled or tracked rovers is typically limited by their physical size, whereas that of hopping rovers is primarily limited by their energy-per-mass ratio, making this approach especially suitable for small systems. Second, they can escape from being stuck. Wheeled and tracked rovers have a tendency to get stuck in loose regolith, and a hopping motion provides an effective means of escape. For example, JAXA deployed the LEV-1 hopping rover to the lunar surface and successfully demonstrated the effectiveness of a small hopping rover[3]. However, hopping performance on regolith, which is common on planetary surfaces, is poor because the regolith absorbs energy during the jump. Therefore, it is necessary to design a hopping mechanism suitable for use on regolith.

The interaction between robots and granular media has been extensively researched. Resistive Force Theory (RFT)[12], an empirical model, is widely applied to simulations of robot locomotion on granular media[13]. The theory was also applied to the design of foot grousers of hopping robots[14]. In the study, diagonal hopping was simulated by means of RFT and optimized grouser shape parameters. While RFT is easily applicable to complex shapes and motions, such as diagonal hopping, it is based on the assumption of quasi-static movement and therefore cannot accurately model dynamic events like hopping motion.

To address such dynamic interactions, Aguilar and Goldman have studied hopping on granular media, proposing a model that includes the added-mass effect and inertial resistance [15].

However, their study focused exclusively on vertical hopping (intrusion), not diagonal hopping, which is inevitable for rovers to move forward. Therefore, understanding the ground interaction during diagonal hopping is of practical importance. The present study expands on this by investigating not only vertical but also diagonal hopping motion, which has not yet been fully explored. The objective of this study is to better understand the dynamic flow induced by hopping motions and how the flow affects the hopping performance, especially during diagonal hopping. This insight will contribute to the design of leg mechanisms that can maintain high hopping performance even on regolith. In this study, we conducted Discrete Element Method (DEM) simulations of hopping motion to directly observe individual particle behavior and gain insights into sand flow dynamics during a hop. The DEM framework also enables us to compute the forces acting on each surface of the intruder (plate) respectively, providing detailed information by separating bulldozing resistance and frictional resistance. Furthermore, by visualizing particle velocities, we can directly identify the shape and size of the added-mass region formed around

[1]Rio Makino is with the Department of Mechanical Systems Engineering, Tokyo University of Agriculture and Technology, Tokyo, Japan. s240506r@st.go.tuat.ac.jp

[2]Takao Maeda is with the Department of Mechanical Systems Engineering, Tokyo University of Agriculture and Technology, Tokyo, Japan. ft8698@me.tuat.ac.jp

978-1-6654-5784-2/26/$31.00 ©2026 IEEE

the intruder, allowing a more comprehensive understanding of the momentum transfer during hopping. Additionally, we conducted a simulation of a hopping robot using the reduced-order observed dynamics and validated the model through comparison with experimental results.

The main contributions of this study are as follows:

- Clarification of the effect of intrusion angle on the dynamic interaction between a plate and granular medium using Discrete Element Method (DEM) simulations, focusing on added mass and effective friction.
- Identification of a trade-off between the effective added mass and the effective friction coefficient that governs hopping performance.
- Experimental validation using a hopping robot, demonstrating that a variable effective friction model reproduces the observed behavior more accurately than a fixed-friction model.

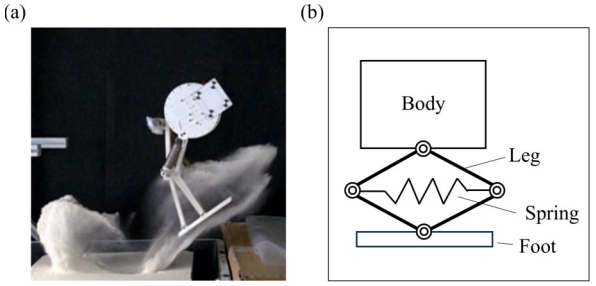

Fig. 1. Hopping robot we are now developing (a) and diamond-shape hopping mechanism (b).

II. METHOD

To better understand the behavior of granular media induced by hopping motion, observation of the granular flow is essential. The present paper applied the Discrete Element Method (DEM) [16] to simulate particle behavior under hopping motion. DEM can directly simulate the effect of microscopic parameters on macroscopic behavior providing deep insights into granular flow. Although the computational cost is high, DEM has been extensively applied to research on granular media for its high reproducibility [17], [18] DEM models the particle contact and calculates each contact (Figure 2).

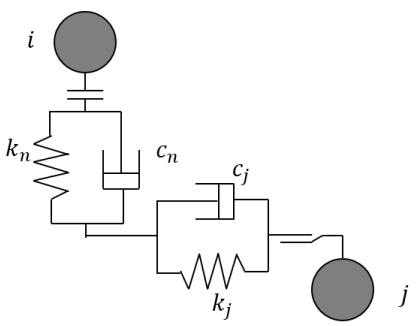

Fig. 2. DEM contact model.

A. Ground Condition

The ground consists of spherical particles. The particle parameters are shown below (Table I). Sphere particles are computationally highly efficient, while it lacks the ability to model real sand shapes. To model the particle shape effect, rolling resistance was applied [19].

TABLE I
PARAMETERS OF PARTICLES

Parameter	Value
Radius	1 mm
Density	2500 kg/m^3
Stiffness	1 GPa
μ (inter particle)	0.45
μ (particle-plate)	0.50
Rolling resistance coefficient	0.15

A granular sample with a low bulk density (porosity of 0.46) was prepared, since lunar regolith tends to have lower density under low gravity, resulting in greater energy loss. This was accomplished by applying high rotational resistance during the packing phase. leading to a more porous structure. The rotational resistance was reset at the beginning of the simulation. Figure 3 shows the comparison of granular beds at low bulk density (used for the simulation) and high bulk density.

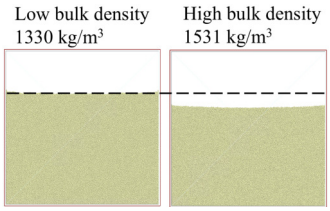

Fig. 3. Adjustment of bulk density.

B. Hopping Simulation

To simulate hopping motion, a time-varying force was applied to a flat plate placed on the granular material. The force profile was defined by a sinusoidal function (Equation 1) to replicate the output of a pantograph-type (diamond-shaped) hopping mechanism (Figure 1(b)) which is commonly used [8], [9]. We conducted simulations for three different force application angles θ: 90, 60, and 30 degrees relative to the horizontal plane. The plate's motion was constrained in all degrees of freedom, except for translation along the axis of the applied force. The maximum force F_{max} and the duration time t_{end} were determined based on experimental hopping motion. The plate measured 150 mm in length and 50 mm in width.

$$F(t) = F_{\text{max}} \sin(\pi t / t_{\text{end}}) \quad (1)$$

TABLE II

PARAMETERS OF SIMULATION

Parameter	Value
θ	90, 30, 60 deg
$F_{\max}$	500 N
t_{end}	0.1 s

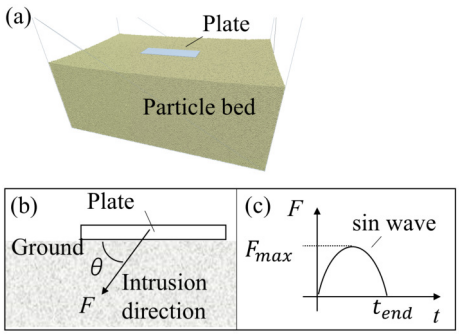

Fig. 4. Modeling of hopping motion. (a) Simulation configuration (b) Simulation parameters (c) Force applied to the plate

C. Application to Simulation

Additionally, we have implemented the friction behavior observed in the DEM simulations into a reduced-order simulation. The model applied inertial resistance, which is proportional to the square of velocity and to permanent deformation, on the basis of spring-damper model. As the friction coefficient differs in response to the intruding angle, we applied a variable friction coefficient that is linearly interpolated. By comparing the simulated result and the experiment of a spring drive hopping robot (Figure 5), we confirmed the validity of the deployment. The robot used a multi-linkage leg consists of two 4-bar linkages, whose kicking force is similar to diamond shaped leg, while much compact. The comparison index was hopping efficiency, which was computed by dividing kinetic energy after takeoff by energy used to hop. The robot suits for testing the model because the robot's foot during the hopping motion change intruding angle while its inclination against horizon change is relatively small. The experiment was conducted three times.

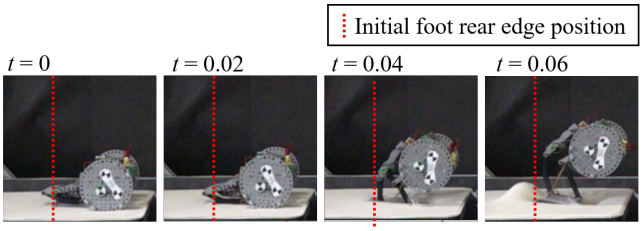

Fig. 5. Experiment with a hopping robot.

III. RESULTS

Figure 6 and Figure 7 show intrusion depth and intrusion speed, respectively. Smaller θ resulted in larger intrusion depth and speed.

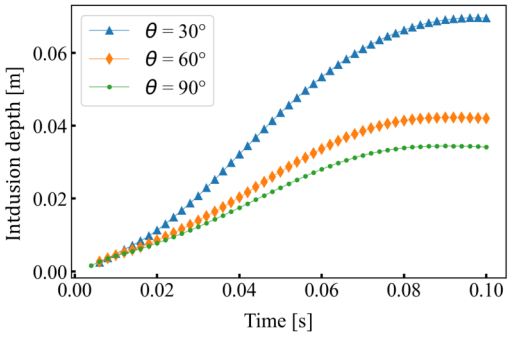

Fig. 6. Intrusion depth of the plate.

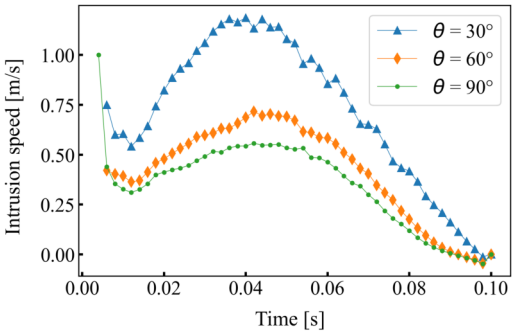

Fig. 7. Intrusion speed of the plate.

The flow behavior of the granular particles is visualized in Figure 8, which shows a snapshot of the particle motion from the simulation. The particles are colored according to their velocity component in the direction of the plate's motion, normalized by the magnitude of the plate velocity ($v_{\text{p-normalized}}$). This normalized velocity, $v_{\text{p-normalized}}$, is an index of how well the particles follow the plate's motion. A value close to 1 (shown in red) means that the particle is moving together with the plate, while a value close to 0 (shown in blue) indicates that it remains stationary. This value is calculated for each particle at every time step using the particle velocity (v_{p}) and the plate velocity (v_{plate}), as defined in Equation (2). Figure 8 show the particle behavior under the condition where the plate intrusion angle was 90, 60, 30 [°] respectively.

$$\boldsymbol{v}_{\text{p-normalized}} = \boldsymbol{v}_{\text{plate}} \cdot \boldsymbol{v}_{\text{p}} / |\boldsymbol{v}_{\text{plate}}|^2 \tag{2}$$

As shown in Figure 8, particles immediately beneath the plate move almost at the same velocity as the plate (colored red or yellow), representing the added mass region. This region becomes thinner and shifts slightly forward as the intrusion angle decreases. In contrast, very few particles are observed above the plate, indicating that the rapid intrusion leaves a cavity that particles cannot refill during the short contact period.

Figure 9 show the normalized velocity fields, separated into vertical and horizontal components, for the 60-degree and 30-degree intrusion cases, respectively.

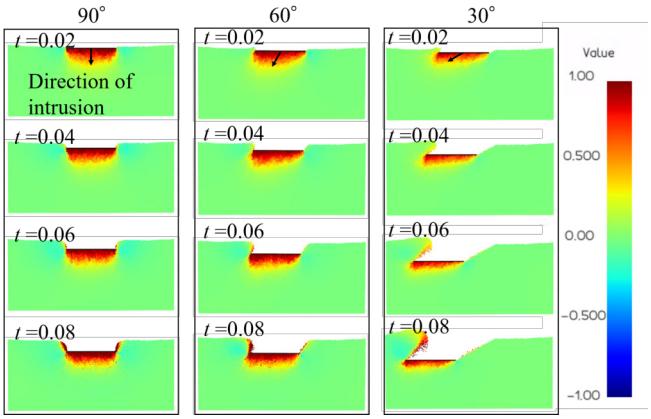

Fig. 8. Normalized particle velocity at each condition. The particle color represents the plate's intruding direction component of the particle velocities, normalized by plate velocity.

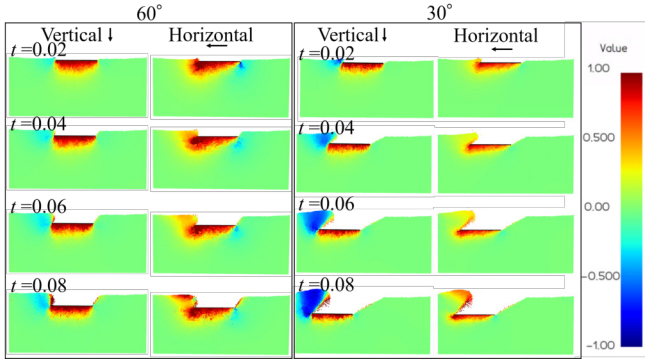

Fig. 9. Vertical and horizontal normalized particle velocity at 60 and 30 degrees. The arrows represent the positive direction of each vertical and horizontal velocity.

Figure 9 compares the normalized vertical and horizontal velocity components for 60° and 30° intrusion angles. In the vertical component, upward-moving particles (blue) appear above the plate, and this upward flow becomes more pronounced at shallower angles (30°). In the horizontal component, particles beneath the plate move forward with it (red), while a backward flow (blue) develops behind the plate, particularly in the 60° case. These observations indicate that diagonal intrusion induces asymmetric particle motion

The effective friction coefficient, calculated using Equation (3), represents the ratio of the tangential to normal force experienced by the plate. Figure 10 shows the temporal evolution of this coefficient for the 60 degree and 30 degree intrusion cases.

Although the material friction coefficient between the particles and the plate was set to 0.5, the effective friction coefficient deviates from this value. Notably, the coefficient is consistently higher for the smaller intrusion angle (30 degrees) than for the larger one (60 degrees). During the main phase of intrusion, the coefficient remains relatively constant before changing as the plate begins to decelerate. During the stable phase, the effective friction coefficient was approximately 0.15 for the 60 degree case, while it showed a higher value of approximately 0.37 for the 30 degree case.

$$\mu = F_{\text{friction}}/N_{\text{bottom}} \tag{3}$$

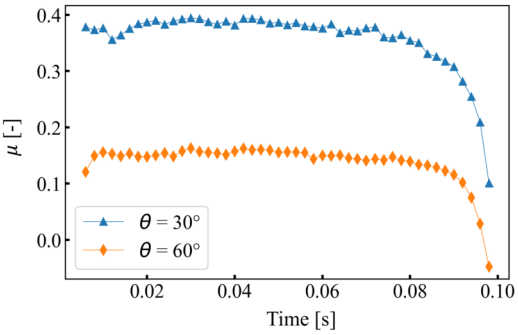

Fig. 10. Evolution of effective friction coefficient.

Figure 11 shows the hopping motion of the simulation with variable friction coefficient and fixed friction coefficient. The foot slips more in the former, and the angle of foot during the intrusion is different. The rear of the foot sinks more in the simulation of fixed friction coefficient while the forward sinks more in the variable friction coefficient. The simulation of variable friction coefficient better reproduces the experiment, especially in terms of slippage amount of the foot (Figure 5). Table III shows the comparison of experiment and simulations. The variable friction coefficient shows better performance compared to fixed friction coefficient.

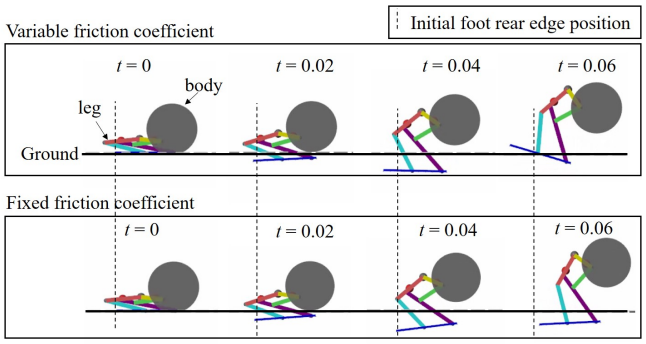

Fig. 11. Hopping robot simulation with variable and fixed friction coefficient.

TABLE III
COMPARISON OF SIMULATION AND EXPERIMENT

Condition	Hopping efficiency [-]
Experiment	0.35±0.01
Sim. (fixed coefficient)	0.46
Sim. (variable coefficient)	0.31

IV. Discussion

From Figure 8, it is observed that the added mass during intrusion is smaller at shallower angles. As the angle becomes shallower, the region of particles moving together with the plate becomes thinner and is also slightly biased toward the front, in the direction of motion.

The decrease in added-mass may be caused by shearing of the sand and slip between sand and plate on the interface. While the movement of plate's normal direction is directly transferred to the particles, the transformation of tangential movement is impeded by sand shearing and slippage.

Added mass is a crucial component of dynamic intrusion, and it affects the reaction force. Since a smaller added mass results in a smaller reaction force, a larger intrusion angle (greater θ) is more effective for hopping.

In addition, the flow in both front and rear of the plate seen in Figure 9 may be caused by the difference in pressure. Particles under high pressure area in front of plate intrusion moved to surrounding region of lower pressure. This flow is also seen at 90 degrees, which is symmetrical. At 60 and 30 degrees, the dominant flow is horizontal in rear and vertical in front. This difference is caused by the diagonal motion of plate. The low pressure region is placed upper in front, while backward in rear. The increase in the effective friction coefficient at shallower intrusion angles can be attributed to the enhanced horizontal interaction between the plate and the granular bed. As the plate moves diagonally, the particles directly beneath it experience forces acting opposite to the plate's direction of motion, originating from both the resistance of the surrounding medium and the inertia of the underlying particles. These opposing forces prevent some of the particles from fully following the plate's horizontal motion, resulting in increased relative slipping at the plate–particle interface. Consequently, the proportion of particles sliding against the plate grows, producing a higher effective friction coefficient. This suggests that the elevated friction observed at shallower angles is primarily governed by the increased horizontal resistance and the resulting slip behavior at the plate surface.

The improved agreement between the simulation and the experiment can be attributed to the introduction of a variable effective friction coefficient that accounts for the dynamic reaction forces during intrusion. By clarifying the relationship between the normal and tangential contact forces under dynamic intrusion conditions as effective friction coefficient, which is an aspect that has not been fully considered in previous studies, the present model captures the dynamic effects more accurately. As a result, this relationship can be regarded as a constitutive representation that better reflects the interaction between the plate and the granular medium during hopping motion.

This study reveals that a key trade-off exists regarding the influence of a hopping leg's intrusion angle on its performance. Specifically, at shallower angles, the added mass decreases, which reduces the inertial resistance when accelerating the leg through the sand. On the other hand, the effective friction coefficient increases, making it easier to generate propulsive force (tangential force) to push off the ground without slipping. This dichotomous relationship suggests the existence not only of a single optimal angle but also of a more complex "optimal kick-off motion." The ultimate goal of this research is to synthetically understand these phenomena to establish a control law governing leg motion and force application that maximizes hopping performance (jump distance and height) for a given energy input. To achieve this, it will be essential for future work to consider the effects of the plate's tilt (orientation) and to systematically investigate how this relationship is affected by other parameters, such as particle shape and friction coefficients. These findings will significantly contribute to the design and operation of exploration rovers on regolith-covered planetary bodies.

V. CONCLUSION

This study investigated the dynamic interaction between a hopping leg and a granular medium using the Discrete Element Method, aiming to provide a physical foundation for designing high-performance planetary rovers.

The key finding is a fundamental trade-off governed by the leg's intrusion angle: shallower intrusion reduces added mass but increases effective friction. This relationship reveals that optimal hopping performance cannot be achieved through a single fixed angle, but rather through a dynamic "kick-off" motion that balances inertial and propulsive requirements.

Incorporating the observed friction behavior into a reduced-order model improved the predictive accuracy of the simulation, suggesting that this relationship can serve as a constitutive component in future dynamic models.

These insights establish a new framework for understanding and predicting leg–terrain interactions in granular environments. Future work should develop quantitative formulations of this trade-off and extend the approach to other locomotion modes such as legged or wheeled motion at high speed. Ultimately, the constitutive relationships identified here lay the groundwork for physically informed control strategies that enable agile and robust locomotion on planetary surfaces.

ACKNOWLEDGMENT

This work was supported by JST Moonshot R&D – MILLENNIA Program Grant Number JPMJMS2238.

References

[1] Shinichiro Sakai, Kenichi Kushiki, Shujiro Sawai, Seisuke Fukuda, Yu Miyazawa, Takayuki Ishida, Kazuki Kariya, Takahiro Ito, Satoshi Ueda, Kentaro Yokota, Taro Kawano, Makiko Ohtake, Kazuto Saiki, Yusuke Nakauchi, Keisuke Michigami, Katsumi Furukawa, Yuki Akizuki, Shusaku Kanaya, Tomihiro Kinjo, Kenta Goto, Kenichiro Sawada, Yoshihide Sugimoto, Hiroshi Takeuchi, Atsushi Tomiki, Hiroyuki Toyota, Taiichi Nagata, Junichi Nakatsuka, Kenichiro Maki, Takahide Mizuno, Hirohide Shiratori, Masaki N. Nishino, Naoto Usami, Junji Kikuchi, Hitoshi Hamori, Ryo Hirasawa, Yusuke Shibasaki, and Hiroaki Saito. Moon landing results of SLIM: A smart lander for investigating the Moon. *Acta Astronautica*, 235:47–54, October 2025.

[2] Kosuke Sakamoto, Toui Sato, Kiyohisa Izumi, Tomoki Kato, Takao Maeda, and Yasuharu Kunii. A Random Walk-Based Stochastic Distributed Exploration Algorithm for Low-Cost Swarm Robots. In *2024 IEEE/SICE International Symposium on System Integration (SII)*, pages 998–1003, January 2024.

[3] Takao Maeda, Yasuharu Kunii, Kotaro Shindori, Masatsugu Otsuki, Kento Yoshikawa, and Tetsuo Yoshimi. Mechanism Design and Action Strategy for Small Hopping Rover. In *Proceedings of the 2017 JSME Conference on Robotics and Mechatronics,*, pages 2P2–A11, Fukushima, Japan,, May 2017.

[4] Tetsuo Yoshimitsu and Takashi Kubota. Engineering Challenges and Results by MINERVA-II Asteroid Surface Rovers. *Journal of the Robotics Society of Japan*, 38(8):754–761, 2020.

[5] Gwang-Pil Jung, Carlos S. Casarez, Jongeun Lee, Sang-Min Baek, So-Jung Yim, Soo-Hwan Chae, Ronald S. Fearing, and Kyu-Jin Cho. JumpRoACH: A Trajectory-Adjustable Integrated Jumping–Crawling Robot. *IEEE/ASME Transactions on Mechatronics*, 24(3):947–958, 2019.

[6] Elliot W. Hawkes, Charles Xiao, Richard-Alexandre Peloquin, Christopher Keeley, Matthew R. Begley, Morgan T. Pope, and Günter Niemeyer. Engineered jumpers overcome biological limits via work multiplication. *Nature*, 604(7907):657–661, April 2022.

[7] Riki Minegisi, Takao Maeda, Kosuke Sakamoto, and Yasuharu Kuni. Discussion of Relationship between Expansion Trajectory of Jumping Mechanism and Mobility Performance. , 40(7):643–646, 2022.

[8] Yanheng Zhang, Lufeng Zhang, Wei Wang, Yangmin Li, and Qingwen Zhang. Design and Implementation of a Two-Wheel and Hopping Robot With a Linkage Mechanism. *IEEE Access*, 6:42422–42430, 2018.

[9] Paolo Fiorini and Joel Burdick. The Development of Hopping Capabilities for Small Robots. *Autonomous Robots*, 14(2/3):239–254, 2003.

[10] Zhihuai Miao, Jixue Mo, Gang Li, Yinghao Ning, and Bing Li. Wheeled hopping robot with combustion-powered actuator. *International Journal of Advanced Robotic Systems*, 15(1):1729881417745608, January 2018.

[11] Mirko Kovač, Manuel Schlegel, Jean-Christophe Zufferey, and Dario Floreano. A miniature jumping robot with self-recovery capabilities. In *2009 IEEE/RSJ International Conference on Intelligent Robots and Systems*, pages 583–588. IEEE, 2009.

[12] Chen Li, Tingnan Zhang, and Daniel I. Goldman. A Terradynamics of Legged Locomotion on Granular Media. *Science*, 339(6126):1408–1412, March 2013.

[13] Hirotaka Suzuki, Kota Katsushima, and Shingo Ozaki. Study on applicability of RFT to traveling analysis of wheel with grousers: Comparison with DEM analysis as a virtual test. *Journal of Terramechanics*, 83:15–24, June 2019.

[14] Kosuke Sakamoto, Masatsugu Otsuki, Takao Maeda, Kent Yoshikawa, and Takashi Kubota. Evaluation of Hopping Robot Performance With Novel Foot Pad Design on Natural Terrain for Hopper Development. *IEEE Robotics and Automation Letters*, 4(4):3294–3301, October 2019.

[15] Jeffrey Aguilar and Daniel I. Goldman. Robophysical study of jumping dynamics on granular media. *Nature Physics*, 12(3):278–283, March 2016.

[16] P. A. Cundall and O. D. L. Strack. A discrete numerical model for granular assemblies. *Géotechnique*, 29(1):47–65, March 1979.

[17] C. J. Coetzee. Calibration of the discrete element method and the effect of particle shape. *Powder Technology*, 297:50–70, September 2016.

[18] H. Nakashima, H. Fujii, A. Oida, M. Momozu, Y. Kawase, H. Kanamori, S. Aoki, and T. Yokoyama. Parametric analysis of lugged wheel performance for a lunar microrover by means of DEM. *Journal of Terramechanics*, 44(2):153–162, April 2007.

[19] C. M. Wensrich and A. Katterfeld. Rolling friction as a technique for modelling particle shape in DEM. *Powder Technology*, 217:409–417, February 2012.